

# Chain Walking: A New Strategy to Control Polymer Topology

Zhibin Guan,\* P. M. Cotts, E. F. McCord, S. J. McLain

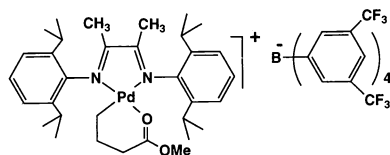
Ethylene pressure has been used to control the competition between isomerization (chain walking) and monomer insertion processes for ethylene coordination polymerization catalyzed by a palladium- $\alpha$ -diimine catalyst. The topology of the polyethylene varies from linear with moderate branching to "hyperbranched" structures. Although the overall branching number and the distribution of short-chain branching change very slightly, the architecture or topology of the polyethylene changes from linear polyethylene with moderate branches at high ethylene pressures to a hyperbranched polyethylene at low pressures.

Vinyl polymers are an important category of synthetic materials—millions of tons are produced every year for broad applications such as fibers, plastics, and elastomers (1). Most vinyl polymers are synthesized by addition polymerization of vinyl monomers. In various addition polymerization mechanisms (anionic, cationic, free radical, group transfer, coordination, and so on), the active growing site usually stays at the chain end, and the unidirectional monomer addition to the chain end leads to the formation of linear polymers (2). The need to synthesize polymers with unusual properties has driven the effort to design polymers with new architectures (3). One approach is to introduce branches into the polymer backbone to produce architectures such as dendritic (4) and its practical analog, the hyperbranched structure (5). Most of the hyperbranched polymers reported are made from condensation polymerization of AB<sub>2</sub> type of monomers, and recently an elegant "self-condensing" approach was applied to polymerize vinyl monomers to give hyperbranched structures (6, 7). In both approaches, branching is introduced by the structure of the monomer. Each addition of a monomer increases the number of active sites from one to two (Fig. 1, A and B). Despite the elegance of these approaches, most of them require the synthesis of a specially designed monomer. It is highly desirable to identify methods that can directly polymerize existing commodity monomers to give controllable architecture. Here we report a fundamentally different approach in which the polyethylene (PE) topology is controlled simply by pressure for ethylene polymerization catalyzed by a palladium (Pd) catalyst.

Our approach is to introduce branching by using a polymerization system in which the active growing site isomerizes to an internal position on the polymer backbone during

propagation, so that the next monomer unit can be assembled onto the polymer backbone instead of at the end (Fig. 1C). Instead of introducing branching by monomer structure, here the branching is introduced by a catalyst that can control the position for the next monomer addition (8). This nonlinear fashion of chain propagation will lead to the formation of branched and hyperbranched polymer.

The system we describe here to demonstrate the concept is ethylene coordination polymerization catalyzed by a Pd- $\alpha$ -diimine complex, a catalyst that was discovered by Johnson *et al.* (9) (Scheme 1).



Scheme 1

For coordination polymerization of ethylene and  $\alpha$ -olefins, reactions such as chain transfer by the  $\beta$ -hydride elimination and isomerization (or chain walking) process compete with propagation (10). Although the chain transfer process has been used extensively to control the molecular weight for olefin polymerization, little work has been done to use the isomerization process to control the polymer topology. For early transition metal catalysts such as Ziegler-Natta and metallocene catalysts, the chain walking rate is usually very small compared to the insertion rate, and the chain growth is linear. Late transition metal catalysts, however, are usually very good at catalyzing alkene isomerization (10). Fink and co-workers have shown that chain walking exists in the polymerization of  $\alpha$ -olefins catalyzed by some nickel catalysts (11). It was recently discovered that  $\alpha$ -diimine complexes of nickel and Pd catalyze the polymerization of ethylene and  $\alpha$ -olefins in which there exists a fast chain walking (9). The variation of pressure, temperature, and catalyst allows access to an ethylene homopolymer whose structure varies from a highly branched,

completely amorphous material to a linear semicrystalline material. Microstructural studies have revealed that the ethylene homopolymer made by the Pd- $\alpha$ -diimine catalyst has many branches, and the simplest form of branch-on-branch, that is, the *iso*-butyl group, was also observed (12). The distinctive microstructure of PE was explained by a mechanism in which chain walking competes with chain propagation (9, 12). These previous studies suggest that the chain walking process might be able to be used to control the polymer topology as well. Our investigation has revealed that the chain walking process can be regulated by ethylene pressure, and thus the PE topology can be controlled from a linear structure with moderate branching to a hyperbranched structure by simply changing the ethylene pressure ( $P_E$ ).

We polymerized ethylene with the Pd catalyst at  $P_E$  ranging from 10.1 to 3447.4 kPa (Table 1) (13). Size exclusion chromatography (SEC) equipped with a refractive index and a multiangle light scattering (MALS) detector was used to measure the weight-averaged molecular weight  $M_w$  and the molecular size (radius of gyration  $R_g$ ) of eluting fractions of polymer with the well-established expressions for classical light scattering:

$$\lim_{c \rightarrow 0} Kc/R_{\Theta} = \frac{1}{M_w} \times [1 + 16\pi^2 n^2 R_g^2 \sin^2(\Theta/2)/3\lambda^2] \quad (1)$$

where  $R_{\Theta}$  is the Rayleigh ratio at scattering angle  $\Theta$ ,  $c$  is the concentration of the polymer, and  $K$  is equal to  $4\pi^2 n^2 (dn/dc)^2 / \lambda^4 N_A$ , with  $n$  being the refractive index of the solvent,  $\lambda$  the wavelength of light,  $N_A$  Avogadro's number, and  $dn/dc$  the refractive index increment (Table 1).

The very high  $M_w$ 's and the relatively narrow polydispersities (the ratio of  $M_w$  to the number-averaged molecular weight  $M_n$ ) indicate a controlled single-site polymerization. We observed that the  $R_g$  for PE samples with similar  $M_w$ 's increased with increasing  $P_E$  (Table 1, entry 1 and 2). Because the online MALS detector measures  $M_w$  and  $R_g$  for every fraction of polymers eluted from the SEC column, we can compare the  $R_g$  at the same  $M_w$  for different samples. In Fig. 2 we compare the angular dependence of the fraction of PE at a  $M_w$  of 400,000 for the three samples that were made at 10.1, 101.3, and 3447.4 kPa. A large difference in the slope was observed, indicating that at the same  $M_w$  the  $R_g$ 's are different. The  $R_g$  at  $M_w = 400,000$  was 30.0, 18.5, and 10.5 nm for the samples polymerized at 3447.4, 101.3, and 10.1 kPa, respectively (a range of a factor of 3 in  $R_g$ ). The separation of the polymer by SEC provides  $R_g$  as a function of  $M$  and as shown in Fig. 3,  $R_g$  consistently shifts upward as  $P_E$  increases.

For a linear flexible polymer forming a

DuPont Central Research, Experimental Station, Wilmington, DE 19880, USA.

\*To whom correspondence should be addressed.

random coil,  $R_g$  scales as  $M^{1/2}$  (14). So, a radius change of a factor of 3 requires nearly an order of magnitude change in  $M$ . The dramatic difference in  $R_g$  for PE samples of the same  $M_w$  indicates that either the degree of branching or the polymer topology changes with  $P_E$ . The size of a polymer molecule changes as the branching level changes; as the amount of branching increases,  $R_g$  usually decreases, because the polymer molecule becomes more compact. The molecular dimension also changes as the polymer topology changes; for example, a dendritic or hyperbranched polymer will be more compact than a linear polymer (15). Without further evidence, two possibilities can account for the observed change of molecular dimension with polymerization pressure: (i) a change in

branching density or (ii) a change in branching topology.

We used quantitative  $^{13}\text{C}$  nuclear magnetic resonance (NMR) to analyze the branching density and short-chain branching distribution for these PE samples. A branch is defined as a unit from a methyl to the nearest methine. The total branches (total methyl) and each of the individual short-chain branches (methyl, ethyl, propyl, butyl, and amyl) were almost constant for the PE samples made at different  $P_E$ 's (Fig. 4). Because the number of total branches stays relatively constant, it is the branching topology that changes with  $P_E$ . We propose that at high  $P_E$ , relatively linear PE with short branches forms; but at low pressure, the PE has many branch-on-branch structures approaching the hyperbranched structure (Fig. 1C).

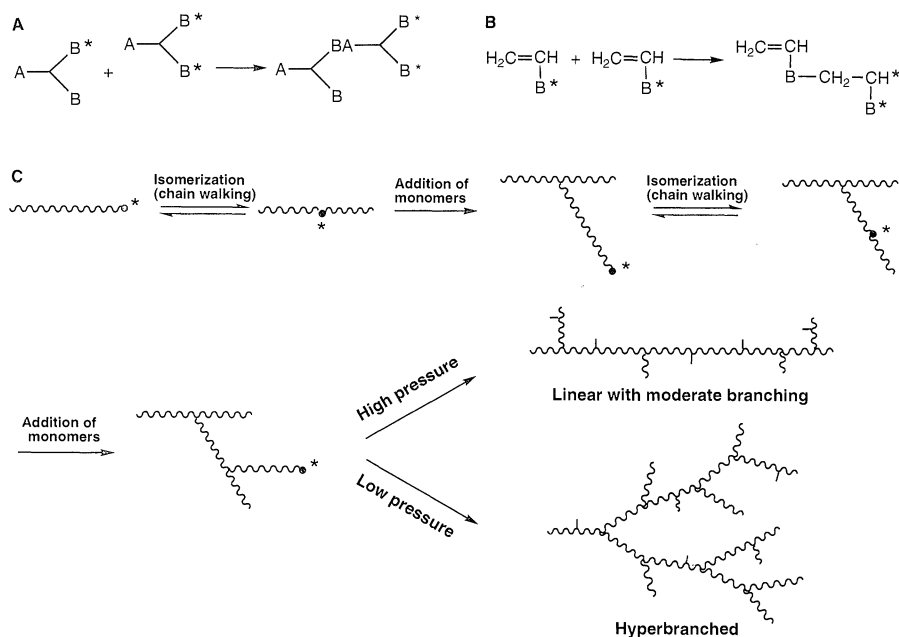


**Fig. 1.** (A) Condensation polymerization of  $\text{AB}_2$  monomers to give a hyperbranched polymer. Condensation of each new monomer increases the active site from one to two. (B) "Self-condensing" polymerization of vinyl monomers to give a hyperbranched polymer. Addition of a new monomer increases the active site from one to two. (C) Proposed new approach to make hyperbranched polymer. The active site isomerizes to the internal backbone, and addition of monomers leads to branching.

**Table 1.** Summary of SEC/MALS, solution viscosity, dynamic light scattering (DLS), and  $^{13}\text{C}$  NMR data on polyethylene samples. SEC/MALS analyses were carried out at  $40^\circ\text{C}$  in tetrahydrofuran (THF) with a flow rate of 0.5 ml/min on two 30-cm columns (Polymer Laboratories Mixed D, 5  $\mu\text{m}$  particle size). The molecular weight and  $R_g$  were obtained with a Wyatt Technology multiangle light scattering detector using 632.8-nm light. The intrinsic viscosity was measured in THF at  $40^\circ\text{C}$ . DLS was done in THF with the Brookhaven Instruments goniometer and a BI9000AT correlator. The data for the two polypropylene samples PP1 and PP2 are from (15). 1B1% is the percentage of methyl branches in *sec*-butyl-ended branches as determined by quantitative  $^{13}\text{C}$  NMR (under the same conditions as described in the caption of Fig. 4).  $\rho$  is the ratio of  $R_g$  over  $R_H$ ; dashes indicate that the data are not available.

Entry	Pressure (kPa)	$M_w$ (SEC/MALS)	$M_w/M_n$ (SEC/MALS)	$R_g$ (nm) (SEC/MALS)	$R_H$ (nm) (DLS)	$\rho \equiv R_g/R_H$	$[\eta]$ (ml/g) (SEC/ $\eta$ )	1B1%
1	10.1	155,000	1.40	6	7.8	0.8	16.9	24.2
2	101.3	480,000	1.57	21.0	16.7	1.3	60.6	21.2
3	3447.4	440,000	1.61	31.8	18.3	1.7	171.4	14.8
PP1	—	189,000	—	—	—	—	133	—
PP2	—	371,000	—	—	—	—	210	—

The simplest branch-on-branch structure—the *sec*-butyl structure—was observed and quantified by  $^{13}\text{C}$  NMR. The *sec*-butyl branch  $\text{RCH}(\text{CH}_3)(\text{CH}_2\text{CH}_3)$  contains both a methyl and an ethyl branch. This subclass of branch-on-branch structures was confirmed by using two-dimensional NMR techniques (12). This unique branching in an ethylene homopolymer appears to be a consequence of the high rate of chain walking relative to olefin insertion (propagation) with the Pd catalyst. The percentage of methyl and ethyl branches incorporated in *sec*-butyl-ended branches shows a definite dependence on ethylene pressure. Both the percentage of ethyl branches in *sec*-butyl-ended branches and the percentage of methyl branches in *sec*-butyl-ended branches increased as a function of decreasing  $P_E$  (Table 1).

Further evidence for a change of PE topology was obtained from hydrodynamic measurements of viscometry and diffusion. The intrinsic viscosity ( $[\eta]$ ) for the three polymers (Table 1) varied considerably with  $P_E$ , from 170 ml/g for the highest pressure polymer with  $M_w$  of 440,000 to 17 ml/g for the lowest pressure polymer with  $M_w$  of 155,000. For polymers of similar structure, this difference in  $M_w$  would result in less than a factor of 2 difference in  $[\eta]$ . Atactic polypropylene of similar  $M_w$  (16) shows a 40% smaller  $[\eta]$  than the highest pressure PE we synthesized, which indicates a sub-

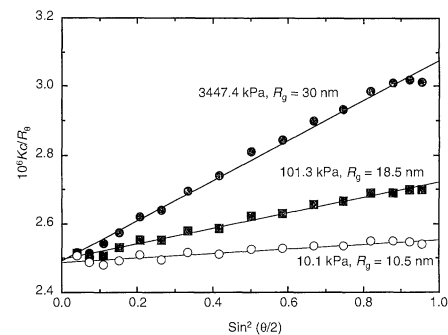


**Fig. 2.** Comparison of Debye plots for the fraction of polymer at  $M_w$  of 400,000 g/mol for the three polyethylene samples made at 10.1, 101.3, and 3447.4 kPa.

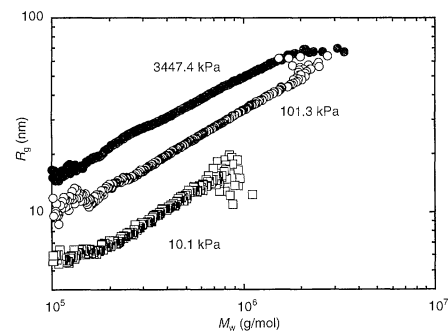


**Fig. 3.** Correlation of  $R_g$  with  $M_w$  for the three polyethylene samples made at 10.1, 101.3, and 3447.4 kPa.

stantial fraction of branches even at high pressure. At the lowest pressure, the measured  $[\eta]$  is reduced nearly an order of magnitude from the expectation for atactic polypropylene of the same  $M_w$ , indicating a highly compact, densely branched polymer.

The limiting translational diffusion coefficient at infinite dilution,  $D_0$ , was also determined for these three polymers (using dynamic light scattering) and converted into a Stokes radius,  $R_H$  (Table 1). Additional evidence for a hyperbranched structure is provided by the ratio  $R_g/R_H$ , which reflects polymer chain architecture and segment density (17) (Table 1). In general, linear flexible polymers exhibit values of  $R_g/R_H$  around 1.5 to 1.7 in good solvents. A value less than unity, 0.78, is predicted for a hard sphere. Experimental results of less than unity have been reported for multiarm stars (18), microgels (19), and dendritic polymers (20). Although our high-pressure polymer has a ratio of 1.7, for the lowest pressure sample this ratio is less than unity.

We use the polymerization mechanism proposed previously (9, 11) to explain our experimental observations (Fig. 5). The basic events during polymerization are the following: ethylene coordination and dissociation, isomerization (chain walking), ethylene insertion, and chain transfer. Because chain transfer only af-

fects  $M_w$  but not the polymer topology, for simplicity it is omitted from the discussion. Chain walking only occurs when ethylene dissociates from the metal center and stops at the catalyst resting state ( $S_1$  and  $S_2$ ); that is, the ethylene-coordinated form of the catalyst.

After ethylene dissociation from the resting state  $S_1$ , the Pd catalyst walks along the polymer chain by means of  $\beta$ -hydride elimination and a readdition process until being trapped by another ethylene to go to another resting state  $S_2$ . Insertion of ethylene at  $S_2$  produces a new branch. The number of carbons ( $n$ ) that the catalyst walks from  $S_1$  to  $S_2$  is the distance between two branches. The walking distance  $n$  should exhibit a statistical distribution governed by the competition between the chain walking and trapping processes. The trapping rate follows first-order dependence on ethylene concentration, or  $P_E$ . At high  $P_E$ , the trapping is fast and therefore the average walking distance is relatively short. The polymer formed has relatively linear topology with moderate branches. At low  $P_E$ , the trapping is slow and the catalyst may walk many carbons before being trapped, leading to the formation of many branches on branches: a hyperbranched topology.

The mechanism also explains why the branching density and the distribution of short chain branches were not sensitive to  $P_E$ . Ac-

cording to Brookhart's kinetic study, the chain walking is much faster than trapping: that is,  $k_W^1, k_W^{-1} \gg k_D, k_T$  (21). In this case, the different chain walking species  $W_1, W_2, W_3, \dots, W_i, \dots, W_n$  may be treated as one single species, and the total rate of chain walking may be expressed as Eq. 2

$$\frac{dS_1}{dt} = k_T\{[W_1] + [W_2] + \dots + [W_n]\} \times [\text{ethylene}] = k_T \sum_{i=1}^n [W_i][\text{ethylene}] \quad (2)$$

where the sum of concentration of  $W_i$  may be expressed by Eq. 3 based on the ethylene association/dissociation equilibrium:

$$\sum_{i=1}^n [W_i] = K_{eq} \frac{[S_1]}{[\text{ethylene}]} \quad (3)$$

Substitution of Eq. 3 into Eq. 2 gives

$$\frac{dS_1}{dt} = k_T K_{eq} [S_1] \quad (4)$$

Thus, the overall chain walking rate is independent of  $P_E$ . Because each chain walking species  $W_i$  will potentially lead to one kind of branching after ethylene trapping and insertion, the pressure independence of the chain walking rate will give constant branching density at various  $P_E$ 's. Because  $k_W^1, k_W^{-1} \gg k_D, k_T$ ,  $P_E$  mainly affects relatively long chain branches and has little effect on very short branches such as methyl, ethyl, propyl, butyl, and amyl. This analysis completely agrees with our  $^{13}\text{C}$  NMR results: The branching density and distribution of short-chain branches are insensitive to ethylene polymerization pressure.

## References and Notes

- H. Ulrich, *Introduction to Industrial Polymers* (Hanser, New York, 1993).
- G. Odian, *Principles of Polymerization* (Wiley, New York, 1991).
- O. W. Webster, *Science* **251**, 887 (1991).
- D. A. Tomalia et al., *Macromolecules* **19**, 2466 (1986); G. R. Newkome et al., *J. Am. Chem. Soc.* **108**, 849 (1986); C. J. Hawker and J. M. J. Fréchet, *J. Chem. Soc. Perkin Trans.* **19**, 2459 (1992).
- Y. H. Kim and O. W. Webster, *J. Am. Chem. Soc.* **112**, 4592 (1990); *Macromolecules* **25**, 5561 (1992); C. J. Hawker, R. Lee, J. M. J. Fréchet, *J. Am. Chem. Soc.* **113**, 4583 (1991).
- J. M. J. Fréchet et al., *Science* **269**, 1080 (1995).
- C. J. Hawker, J. M. J. Fréchet, R. B. Grubbs, J. Dao, *J. Am. Chem. Soc.* **117**, 10763 (1995).
- In high-pressure free radical polymerization of ethylene, radical sites may be generated occasionally inside of polymer chains by chain transfer to polymer chains [T. Usami and S. Takayama, *Macromolecules* **17**, 1756 (1984)]. However, the mechanism is completely different from the one discussed in this report, and the random radical chain transfer process cannot be regulated to control polymer topology.
- L. K. Johnson, C. M. Killian, M. Brookhart, *J. Am. Chem. Soc.* **117**, 6414 (1995).
- J. P. Collman et al., *Principles and Applications of Organotransition Metal Chemistry* (University Science Books, Mill Valley, CA, 1987).

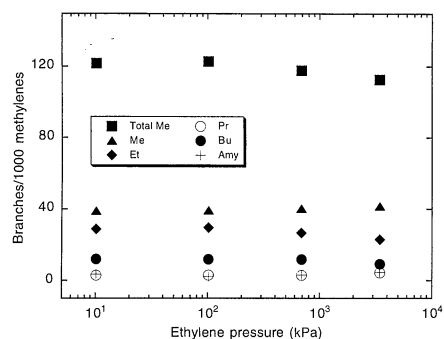


**Fig. 4.**  $^{13}\text{C}$  NMR data on the total number of branches and the distribution of short-chain branches. 100 MHz  $^{13}\text{C}$  NMR spectra were obtained on a Varian Unity 400 MHz spectrometer in a 10-mm probe on 20 weight% solutions of the polymers and 0.05 M CrAcAc in 1,2,4-trichlorobenzene unlocked at 120° to 140°C using a 90° pulse of 17.8  $\mu\text{s}$ , a spectral width of 35 kHz, a relaxation delay of 5 s, an acquisition time of 0.64 s, and inverse gated decoupling. Integrals of characteristic carbons in each branch were measured and reported as number of branches per 1000 methylenes (including methylenes in the backbone and branches). Me, methyl; Et, ethyl; Pr, propyl; Bu, butyl; Amy, amyl.

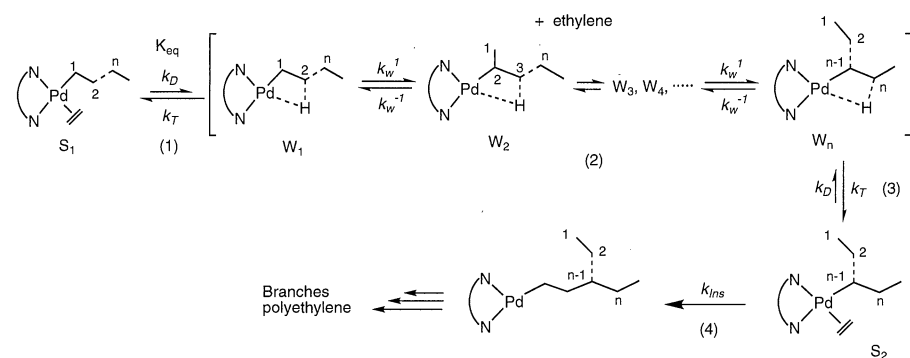


**Fig. 5.** Mechanistic model for ethylene polymerization catalyzed by the Pd- $\alpha$ -diimine catalyst. Individual kinetic steps are (1) dissociation of ethylene, (2) isomerization (chain walking), (3) association of ethylene (trapping), and (4) insertion of ethylene.  $K_{eq}$  is the equilibrium constant for ethylene dissociation-association;  $k_D$ ,  $k_T$ , and  $k_{ins}$  are the rate constants for ethylene dissociation, trapping, and insertion, respectively;  $k_W^1$  and  $k_W^{-1}$  are the rate constants for forward and backward chain walking.

11. V. M. Möhring and G. Fink, *Angew. Chem. Int. Ed. Engl.* **24**, 1001 (1985).
12. S. J. McLain *et al.*, *Polymer Prep.* **38** (no. 1), 772 (1997).
13. A typical polymerization was done as follows: A solution of 50 mg (33.9  $\mu\text{mol}$ ) of the Pd- $\alpha$ -dimine catalyst in 100 ml of chlorobenzene was transferred into a 600-ml Parr pressure reactor under nitrogen. The reactor was heated to 35°C, and the solution was stirred by a mechanical stirrer set at 500 rpm. The reactor was pressurized with ethylene to 101.3 kPa. Polymerization was continued at 35°C and 101.3 kPa for 18.7 hours. After termination of the polymerization, the solution was diluted with toluene, then passed through a column packed with alumina, silica gel, and Celite to remove the catalyst, and finally precipitated into a large excess of methanol. The polymer was collected and dried in vacuo to give 15.8 g of PE as viscous oil.
14. P. J. Flory, *Principles of Polymer Chemistry* (Cornell Univ. Press, Ithaca, NY, 1953).
15. D. A. Tomalia, A. M. Naylor, W. A. Goddard III, *Angew. Chem.* **102**, 119 (1990).
16. Z. Xu *et al.*, *Macromolecules* **18**, 2560 (1985).
17. W. Burchard, *Adv. Polym. Sci.* **48**, 1 (1983).
18. B. J. Bauer, L. J. Fetters, W. W. Graessely, N. Hadjichristidis, G. F. Quack, *Macromolecules* **22**, 2337 (1989).
19. D. Kunz, A. Thurn, W. Burchard, *Polym. Coll. Sci.* **261**, 635 (1983).
20. R. Scherrenberg *et al.*, *Macromolecules* **31**, 456 (1998).
21. M. S. Brookhart, D. J. Tempel, L. K. Johnson, unpublished data.
22. We thank M. S. Brookhart, L. K. Johnson, M. Spinu, S. D. Ittel, L. Wang, Z. Yang, P. Soper, and S. D. Arthur for helpful discussions; R. E. Fuller for viscosity measurements; and J. Chen, J. Galperin, P. A. Ware, C. A. Urbston, and M. J. Halfhill for technical assistance.

18 November 1998; accepted 17 February 1999

## Hydrogen Peroxide on the Surface of Europa

R. W. Carlson,<sup>1\*</sup> M. S. Anderson,<sup>1</sup> R. E. Johnson,<sup>2</sup> W. D. Smythe,<sup>1</sup>  
A. R. Hendrix,<sup>3</sup> C. A. Barth,<sup>3</sup> L. A. Soderblom,<sup>4</sup> G. B. Hansen,<sup>5</sup>  
T. B. McCord,<sup>5</sup> J. B. Dalton,<sup>6</sup> R. N. Clark,<sup>6</sup> J. H. Shirley,<sup>1</sup>  
A. C. Ocampo,<sup>1</sup> D. L. Matson<sup>1</sup>

Spatially resolved infrared and ultraviolet wavelength spectra of Europa's leading, anti-jovian quadrant observed from the Galileo spacecraft show absorption features resulting from hydrogen peroxide. Comparisons with laboratory measurements indicate surface hydrogen peroxide concentrations of about 0.13 percent, by number, relative to water ice. The inferred abundance is consistent with radiolytic production of hydrogen peroxide by intense energetic particle bombardment and demonstrates that Europa's surface chemistry is dominated by radiolysis.

The composition of a planetary surface is an important indicator of its evolution and subsequent chemical alteration. Europa's surface composition can be modified by extrusion of material from the interior (1), the infall of cometary and meteoritic material, photochemical processes, and by the deposition of material from the magnetosphere (2, 3). Europa is subjected to intense bombardment by jovian magnetospheric particles—energetic electrons, protons, sulfur ions, and oxygen ions (4)—that could alter the composition through radiolysis (5, 6). The relative importance of these chemical alteration processes has not been established for Europa.

Spectra of Europa indicate a water-ice surface (7) with sulfur dioxide (SO<sub>2</sub>) (2, 8) and hydrated minerals (9). The SO<sub>2</sub> could be produced by sulfate decomposition (10) or from implanted sulfur ions (2). The hydrated miner-

als may be evaporite salts (9), from brine extruded from a hypothetical subsurface ocean (11). Infrared (IR) spectra of Europa obtained by Galileo's near-infrared mapping spectrometer (NIMS) (12) showed absorption features (13) at wavelengths of 4.25, 4.03, and 3.50  $\mu\text{m}$ . Carbon dioxide and SO<sub>2</sub> were identified (13) as the 4.25- and 4.03- $\mu\text{m}$  absorbers, similar to previous findings for Ganymede and Callisto (14). We show here that the 3.50- $\mu\text{m}$  feature, corroborated with laboratory measurements and Galileo ultraviolet spectrometer (UVS) (15) data, indicates the presence of hydrogen peroxide (H<sub>2</sub>O<sub>2</sub>), formed in this environment by energetic plasma irradiation of Europa's surface (6).

NIMS reflectance spectra (Fig. 1A) of Europa's leading anti-jovian quadrant (16) show characteristic features of water frost and a feature at 3.50  $\mu\text{m}$  that is not due to H<sub>2</sub>O. Hydrocarbons and ammonium-containing minerals were suggested to account for this feature (13), but such identifications are problematic because their absorption wavelengths do not match that observed, and both classes of compounds exhibit additional, stronger absorption features not evident in the NIMS spectra. For example, methanol (17) shows an absorption band at 3.53  $\mu\text{m}$  and four other strong bands at 3.38, 3.35, 3.14, and 3.04  $\mu\text{m}$  that are not apparent in Europa's spectrum (Fig. 1A). Similar arguments rule out other simple hydrocarbons and ammonium-bearing minerals (18). A more like-

ly candidate for the 3.50- $\mu\text{m}$  feature is H<sub>2</sub>O<sub>2</sub>, which produces 2 $\nu_2$ ,  $\nu_2 + \nu_6$ , and 2 $\nu_6$  combination-bending-mode absorption (19, 20) at  $\sim$ 3.5  $\mu\text{m}$  and has been predicted to occur on icy satellite surfaces (6).

For comparison to the NIMS data, we measured (21) the diffuse reflectance of H<sub>2</sub>O<sub>2</sub> mixtures in water ice and found a band at 3.504  $\mu\text{m}$  (Fig. 1B). Previous measurements (22) of UV-photolyzed, 10 K water ice showed the H<sub>2</sub>O<sub>2</sub> feature at 3.509  $\mu\text{m}$ , and it shifts to 3.505  $\mu\text{m}$  at 70 K. These wavelengths are consistent with the Europa feature (3.50  $\pm$  0.015  $\mu\text{m}$ ). The widths of the Europa and laboratory feature are also consistent, both being  $\sim$ 0.06  $\mu\text{m}$  wide (full width at half maximum) (Fig. 1). With the exception of this feature, frozen aqueous H<sub>2</sub>O<sub>2</sub> solutions produce near-IR spectra that are indistinguishable from those of pure water ice.

An estimate of the surface concentration of H<sub>2</sub>O<sub>2</sub> is obtained by laboratory IR-reflectance measurements of frozen H<sub>2</sub>O<sub>2</sub>-H<sub>2</sub>O solutions at various concentrations (21). Comparing the relative band depths of these spectra with the NIMS spectrum, we find a concentration on Europa of  $\sim$ 0.13  $\pm$  0.07% (by number of H<sub>2</sub>O<sub>2</sub> molecules, relative to H<sub>2</sub>O; this convention is used throughout) (21). The estimate pertains to Europa's 3.5- $\mu\text{m}$ -wavelength, optically sensed surface layer, which is limited by water spectral absorption to depths of about the ice-grain size (23), ignoring porosity. The grain size ( $\sim$ 60  $\mu\text{m}$ ) was determined with the observed IR reflectance factor (24) and radiative-transfer calculations for ice-grain surfaces (25).

Condensed H<sub>2</sub>O<sub>2</sub> in Europa's surface may exist as a solid-state solution in ice or as crystals of pure H<sub>2</sub>O<sub>2</sub> or H<sub>2</sub>O<sub>2</sub>·2H<sub>2</sub>O (20). However, the wavelength (3.52  $\mu\text{m}$ ) of the crystalline phases (at 4 and 80 K) is larger than the wavelength of Europa's feature and outside the range allowed by the estimated wavelength uncertainty. Pure amorphous H<sub>2</sub>O<sub>2</sub> is precluded because its absorption band occurs at 3.56  $\mu\text{m}$  (20).

Hydrogen peroxide absorbs UV radiation (26), so if our identification is correct we expect (6) a corresponding absorption signature to be present in Galileo UVS spectra (27). Disk-resolved UVS measurements (obtained concurrently with the NIMS observations) were com-

<sup>1</sup>Jet Propulsion Laboratory, California Institute of Technology, Pasadena, CA 91109, USA. <sup>2</sup>Engineering Physics, University of Virginia, Charlottesville, VA 22903-2442, USA. <sup>3</sup>Laboratory for Atmospheric and Space Physics, University of Colorado, Boulder, CO 80309-0590, USA. <sup>4</sup>United States Geological Survey, Flagstaff, AZ 86001, USA. <sup>5</sup>Planetary Geosciences Division, University of Hawaii, Honolulu, HI 96822, USA. <sup>6</sup>United States Geological Survey, Denver, CO 80225, USA.

\*To whom correspondence should be addressed at Mail Stop 183-601, Jet Propulsion Laboratory, 4800 Oak Grove Drive, Pasadena, CA 91109, USA. E-mail: rcarlson@lively.jpl.nasa.gov